Improved POCS-based image reconstruction from irregularly-spaced samples

Ryszard Stasiński
Institute of Electronics and Telecommunications, Technical University of Poznań
Piotrowo 3A, PL-60-965 Poznań, Poland, rstasins@et.put.poznan.pl

Janusz Konrad
Department of Electrical and Computer Engineering, Boston University
8 Saint Mary's Street, Boston, MA 02215, USA, jkonrad@bu.edu

ABSTRACT

This paper presents an enhanced POCS-based (projection onto convex sets) method for the reconstruction of a regularly-sampled image from its irregularly-spaced samples. Such a reconstruction is often needed in image processing and coding, for example when using motion compensation. The proposed approach applies two operators sequentially: bandwidth limitation and sample substitution, and is based on our earlier work. The contribution of this paper is a new, simpler implementation of the algorithm that allows for faster convergence, and provides better performance, although at the cost of increased memory requirements.

1 Introduction

Interpolation of intensity from a set of known samples is a common task in image processing and coding. The grids of unknown and known samples can each be defined as a *regular* (periodic) or *irregular* sampling structure (grid). There are 4 scenarios for sampling grid combinations of unknown/known samples:

1. regular→regular - simplest case where interpolation filters are space-invariant; for example, interpolating filters in typical image up-conversion,
2. regular→irregular - more difficult case where interpolation filters are space-variant since samples to be recovered have varying positions with respect to the regularly-spaced known samples; for example, bilinear or bicubic interpolation [1] in *backward* motion compensation in video coding,
3. irregular→regular - still more difficult case where interpolation filters are space-variant but may not be easily specified in general case; for example, *forward* motion-compensation in advanced video coding/interpolation,
4. irregular→irregular - the most general case for which applications have not clearly emerged yet.

The first two cases have been extensively treated in the literature and have found numerous practical applications in image processing and coding. The irregular→regular interpolation has been explored to a lesser degree. The primary reason for this are difficulties associated with the extension of Shannon's sampling theory to signals defined over irregular sampling grids; alternative methods must be found to reconstruct or approximate the original continuous signal.

Although some results on the reconstruction of band-limited functions from their irregularly-spaced samples are available (e.g., [2]), their usefulness in the case of motion-compensated video coding or interpolation is quite limited; theoretically derived constraints on the maximum spacing of irregular samples under the perfect reconstruction condition cannot be satisfied in practice by arbitrarily-distributed image samples after motion compensation. By relaxing the perfect reconstruction condition, other methods were proposed such as the polynomial interpolation or iterative reconstruction [3].

In this paper, we extend our earlier approach to irregular→regular interpolation [5, 6] that is based on *projections onto convex sets* (POCS) [4]. Our new method differs in implementation that is simpler, converges faster and provides better PSNR performance, although at the cost of increased memory requirements.

2 Proposed approach

Let $g = \{g(\mathbf{x}), \mathbf{x} = (x,y)^T \in R^2\}$ be a continuous 2-D projection of the 3-D world onto an image plane and let $g_\Lambda = \{g(\mathbf{x}), \mathbf{x} \in \Lambda\}$ be a discrete image obtained from g by sampling over a lattice Λ [7]. Let's assume that g is band-limited, i.e., $G(\mathbf{f}) = \mathcal{F}\{g\}=0$ for $\mathbf{f} \notin \Omega$ where $\mathcal{F}$ is the Fourier transform, $\mathbf{f} = (f_1, f_2)^T \in R^2$ is a frequency vector and $\Omega \subset R^2$ is the spectral support of g. If the lattice Λ satisfies the multi-dimensional Nyquist criterion [7], the Shannon sampling theory allows to perfectly reconstruct g from g_Λ. However, in the case of irregular sampling the theory is not applicable. Therefore, the general goal is to develop a method for the reconstruction of g from an irregular set of samples $g_\Psi = \{g(\mathbf{x}_i), \mathbf{x}_i \in \Psi \subset R^2, i = 1, ..., K\}$, where Ψ is an irregular sampling grid.

2.1 POCS-based reconstruction algorithm

We use the POCS methodology [4] to reconstruct image g. This methodology involves a set theoretic formulation, i.e., finding a solution as an intersection of property sets rather than by a minimization of a cost function. We use the following sets [5]:

- A_0 - set of all images g such that at $\mathbf{x}_i \in \Psi$, $i = 1, ..., K$ (irregular sampling grid) $g(\mathbf{x}_i) = g_\Psi(\mathbf{x}_i)$,
- A_1 - set of all band-limited images g, i.e., such that $G(\mathbf{f}) = 0$ for $\mathbf{f} \notin \Omega$.

Let the membership in A_0 be assured by a sample replacement operator $\mathcal{R}$ (to enforce proper values on Ψ), while the membership in A_1 – by suitable bandwidth limitation $\mathcal{B}$ (low-pass filtering). Then, the iterative reconstruction algorithm can be expressed as follows:

$$\begin{aligned} g^{k+1} &= \mathcal{B}\mathcal{R}g^k = \mathcal{B}[g^k + \mathcal{S}_\Psi(g - g^k)] \\ &= \mathcal{R}\mathcal{B}g^k = \mathcal{B}g^k + \mathcal{S}_\Psi(g - \mathcal{B}g^k), \end{aligned} \quad (1)$$

where g^k is the reconstructed image after k iterations and $\mathcal{S}_\Psi$ is a sampling operator that extracts image values (luminance/color) on the irregular grid Ψ. Note that equation (1), proposed in [8], results in an approximation rather than interpolation of g_Ψ; the last step is that of low-pass filtering. In order to implement equation (1) on a computer, a suitable discretization must to be applied. In [8], equation (1) was implemented with:

$$g_\Lambda^{k+1} = \mathcal{B}[g_\Lambda^k + \alpha\mathcal{I}_{\Psi/\Lambda}(g_\Psi - \tilde{g}_\Lambda^k)], \quad (2)$$

where the lowpass filtering $\mathcal{B}$ is implemented over Λ and α is a parameter that allows the control of convergence and stability of the algorithm. The symbol $\tilde{g}_\Lambda^k$ denotes a bilinearly-interpolated image g_Λ^k needed to recover image samples on Ψ. Also, note that an interpolation function $\mathcal{I}_{\Psi/\Lambda}$ replaces the sampling operator $\mathcal{S}_\Psi$. This function interpolates image samples $(g_\Psi - \tilde{g}_\Lambda^k)$ defined on Ψ in order to recover samples on Λ. Sauer and Allebach have studied three interpolators $\mathcal{I}_{\Psi/\Lambda}$: one derived from bilinear interpolation and two based on triangulation with planar facets [8]. The implementation (2) of the reconstruction algorithm (1) suffers from two deficiencies. First, by processing all images on Λ there is little flexibility in shaping the spectrum of g_Λ^k; any practical lowpass filtering on Λ must suppress high frequencies since a slow roll-off transition band must be used to minimize ringing on sharp luminance/color transitions. Secondly, the interpolation operator $\mathcal{I}_{\Psi/\Lambda}$, especially the one based on triangulation (better performance), is involved computationally.

In our earlier work [5], we proposed an alternative implementation of (1). Since our goal is the reconstruction of image samples obtained from motion or disparity compensation, a 1/2-, 1/4- or 1/8-pixel precision of motion or disparity vectors is usually sufficient. Therefore, we have proposed to implement (1) on an oversampled grid matching that precision:

$$g_{\Lambda_P}^{k+1} = \mathcal{B}[g_{\Lambda_P}^k + \alpha\mathcal{S}_{\Psi/\Lambda_P}(g_{\Psi/\Lambda_P} - g_{\Lambda_P}^k)], \quad (3)$$

where $\mathcal{B}$ is implemented on Λ_P, a $P \times P$-times oversampled lattice, and P equals 2, 4, or 8 depending on motion/disparity vector precision. Clearly, Λ is a sub-grid of Λ_P, i.e., $\mathbf{x} \in \Lambda \Rightarrow \mathbf{x} \in \Lambda_P$. g_{Ψ/Λ_P} is the nearest-neighbor interpolation of g_Ψ on Λ_P, defined at each $\mathbf{x}_i \in \Psi$ as follows:

$$g_{\Psi/\Lambda_P}(\mathbf{y}) = \begin{cases} g_\Psi(\mathbf{x}_i) & \text{if } \|\mathbf{x}_i - \mathbf{y}\| \le \|\mathbf{x}_i - \mathbf{z}\|, \\ 0 & \text{otherwise.} \end{cases} \quad (4)$$

with $\mathbf{y}, \mathbf{z} \in \Lambda_P$. Similarly, $\mathcal{S}_{\Psi/\Lambda_P}$ denotes the nearest-neighbor sampling, i.e., sampling on $\mathbf{y} \in \Lambda_P$ that is nearest to $\mathbf{x}_i \in \Psi$. In other words, the implementation (3) is performed on a denser lattice Λ_P and the positions of the irregular samples from Ψ are quantized to the nearest position on Λ_P. This allows us to avoid the cumbersome interpolation $\mathcal{I}_{\Psi/\Lambda}$ under the assumption that a suitable value of P is selected.

2.2 Adaptation of the relaxation coefficient

The choice of the relaxation coefficient α in equation (3) has a direct impact on the convergence properties of the algorithm; the greater the α, the faster the convergence up to some α_{max} above which the algorithm becomes unstable. Experimental results indicate that the value of α_{max} in (3) is closely related to the properties of Ψ; the algorithm tends to diverge in image regions where the number of irregular samples per unit area is highest. To address this we have introduced an α-correcting term:

$$g_{\Lambda_P}^{k+1} = \mathcal{B}[g_{\Lambda_P}^k + (\alpha/d_\Psi)\mathcal{S}_{\Psi/\Lambda_P}(g_{\Psi/\Lambda_P} - g_{\Lambda_P}^k)], \quad (5)$$

where d_Ψ are samples of a function d describing local density of Ψ. The introduction of d_Ψ allows higher values of α_{max}, and therefore faster convergence, than those based on formulation (3). To be a good descriptor of the local grid density, the function d should equal 1 where Ψ is regular, should be greater than 1 in areas where Ψ is denser than Λ, and less than 1 when converse is true. A new, simplified computation of d is described below.

2.3 New implementation

In our original implementation [5], the lowpass filtering was executed in the frequency domain by means of FFT. Here, we propose an alternative simpler implementation using standard filtering operations in *Matlab*, and also a simpler computation of grid density d_Ψ.

2.3.1 Lowpass filtering operator

Properties of the low-pass filter implementing the $\mathcal{B}$ operator are crucial for the algorithm's performance. Let's assume for now that the relaxation parameter α is 0.

Then, algorithm (5) degenerates to repetitive filtering of the initial data set. In the frequency domain, such a repetitive filtering results in amplifying the signal at frequencies where filter's magnitude response is greater than 1, and attenuating – where this response is less than 1. By expressing (5) for α=0, as $g^{k+1}_{\Lambda_P} = \mathcal{B}g^k_{\Lambda_P} + \epsilon$, where ϵ is a correction term, we see the compositing effect of the operator $\mathcal{B}$. In order to assure that the iterations not diverge, we require that the gain of the filter not exceed 1.0 and thus we formulate the first constraint on the low-pass filter $\mathcal{B}$:

$$|H(\omega)| \leq 1, \quad \forall\omega. \tag{6}$$

The above constraint assures that image samples do not get amplified as the iterations progress.
At the same time, it is desirable that the magnitude response $|H(\omega)|$ in the passband be equal to 1.0 or very close to it; this is in order that the correction term in (5) need not compensate for the attenuation of past $g^k_{\Lambda_P}$ (recall that $g^{k+1}_{\Lambda_P} = \mathcal{B}g^k_{\Lambda_P} + \epsilon$). This is particularly important for the DC component of an image. Hence, we require that:

$$|H(0)| = 1. \tag{7}$$

Clearly, the frequency response of the filter has a (local) maximum at $\omega = 0$. At a first glance, it seems that the degree of attenuation in the stopband is not critical due to the effect of repetitive filtering. Experiments show, however, that good attenuation is important for the removal of high-frequency components of recent correction terms in (5). It appears that for best results the error weights in the passband and stopband of the Remez exchange algorithm (design of equiripple FIR filters) should be approximately the same.

2.3.2 Local grid density function

In our previous work [6], we have observed that the precise functional form of the local density grid function d has little influence on the performance of the whole algorithm. This suggests that a simplified (and, perhaps, more efficient) definition should work as well. We propose here to compute the function d by smoothing out (or spreading) the following indicator function (4):

$$\vartheta(\mathbf{x}) = sign\{g_{\Psi/\Lambda_P}(\mathbf{x})\}, \qquad \mathbf{x} = [x, y]^T \in \Lambda_P$$

i.e., function that is equal to 1.0 at nearest-neighbor (Λ_P) positions from Ψ, and zero otherwise. The smoothing filter should have non-negative impulse response, as the local density function cannot be negative, and should retain the signal energy. As the prototype filter, we have used the following impulse response: $h_i(x) = [0.05, 0.17, 0.56, 0.17, 0.05]$, described earlier in [6]. The overall filter is defined as follows: $h(x) = P^2 h_1(x) * h_2(x) * ... * h_P(x)$, where $*$ is the convolution operator (P-fold self-convolution times suitable gain). This 1-D horizontal filter is convolved with its transposed (vertical) sibling to obtain a separable 2-D FIR filter. The density grid function d is therefore obtained by the following filtering:

$$d(x, y) = \vartheta(x, y) * h(x) * h(y), \quad \mathbf{x} = [x, y]^T \in \Lambda_P,$$

based on which d_Ψ can be computed. To avoid problems with divisions by zero in (5), all "unused" samples of the resulting density grid function, i.e., not coinciding with (quantized) positions in Ψ, have been set to 1.0.

3 Experimental results

The proposed method was implemented in *Matlab*, and tested on a pair of ITU-R 601 (720×480) stereoscopic images *Flower* (Fig. 1). Disparity-compensated prediction was applied to the left image in order to reconstruct the right image; disparity vectors predict the right image on an irregular grid to which the proposed algorithm is applied. Reconstruction error is used to gauge algorithm's performance [6]. The algorithm was tested for the oversampling ratio $P = 4$.
The lowpass filters have been designed using the Remez exchange algorithm for linear-phase equiripple FIR filters. Although the method allows an easy determination of band edges and proportions between ripples in passband and stopband, there is no direct way to impose a constraint that filter frequency response have a maximum at $\omega = 0$. Since this constraint is crucial to algorithm's performance, it has been enforced manually by tuning error weights in both filter bands, and by slightly modifying band edges, originally set to $0.78/P$ and $1.22/P$ (i.e., the same as in [5, 6]). The resulting filter coefficients have been normalized (divided by their sum, i.e., by $H(0)$). The constraint (6) has been enforced manually as well (trial-and-error).
We have designed various filters of which results for 11-, 19-, and 27-tap filters are presented here. For 19-tap filters the new method has similar computational complexity on 720×480-pixel images as the original method based on frequency-domain filtering [5, 6]. Fig. 2 (top) shows the evolution of the reconstruction error PSNR for the 11- and 27-tap filters, as well as for the frequency-domain filtering proposed earlier [6]. In the case of carefully-designed FIR filters, $\alpha = 0.8$ allowed a stable evolution, while for frequency-domain filtering α had to be limited to 0.7. The weights of passband and stopband errors were $[1, 1]$, while band edges – as stated above. As can be seen, in early iterations the frequency-domain filter performs better, but after 4 iterations the roles are reversed; the new filters assure faster convergence of the reconstruction algorithm. The final PSNR for the 11-tap filter is slightly lower than that for the 27-tap filter. This is due to a relatively large ripple in the passband of the 11-tap filter, thus resulting in a stronger signal attenuation at the bandwidth edge.
Fig. 2 (bottom) compares the performance of 11- (band error weights $[1, 1]$, and $[1, 10]$), 19- (band error weights

Figure 1: Right image of stereo pair *Flower*.

[4, 1]), and 27-tap filters. An 11-tap filter with $[10, 1]$ weights was unstable, and a 19-tap filter with $[1, 1]$ weights has a minimum at $\omega = 0$. The 11-tap filter with $[1, 10]$ weights (denoted "FIR - 2") has a particularly large ripple in the passband, hence, introduces strong attenuation at the passband edge, and poor final PSNR. The high-quality filters of length 19 and 27 have the smallest ripples. Fig 2.b also shows that the size of ripples in the stopband determines the convergence speed of the algorithm; the 19-tap filter has relatively large ripples. The 11-tap filter with $[10, 1]$ weights did not converge at all. Interestingly, a strong attenuation in the passband (actually, reduced bandwidth) of the second 11-tap filter increases algorithm's stability; α's as large as 1.6 do not cause any convergence problems, although the steady-state PSNR is not as high as for other filters.

4 Conclusion

We have presented a simplified implementation of irregular→regular image interpolation based on POCS methodology. The new implementation is simple and can be easily programmed in *Matlab*, assures faster convergence, and lower reconstruction errors. The price to be paid for the implementation simplicity and improved performance are increased memory requirements to store a $P \times P$-oversampled lattice.

References

[1] R.G. Keys, "Cubic convolution interpolation for digital image processing," *IEEE Trans. Acoust. Speech Signal Process.*, vol. 29, no. 6, pp. 1153–1160, Dec. 1981.

[2] H. Feichtinger and K. Gröchenig, "Theory and practice of irregular sampling," in *Wavelet: Mathematics and Applications*, J. Benedetto and M. Frazier, Eds., chapter 8, pp. 305–363. CRC Press, Boca Raton FL, 1994.

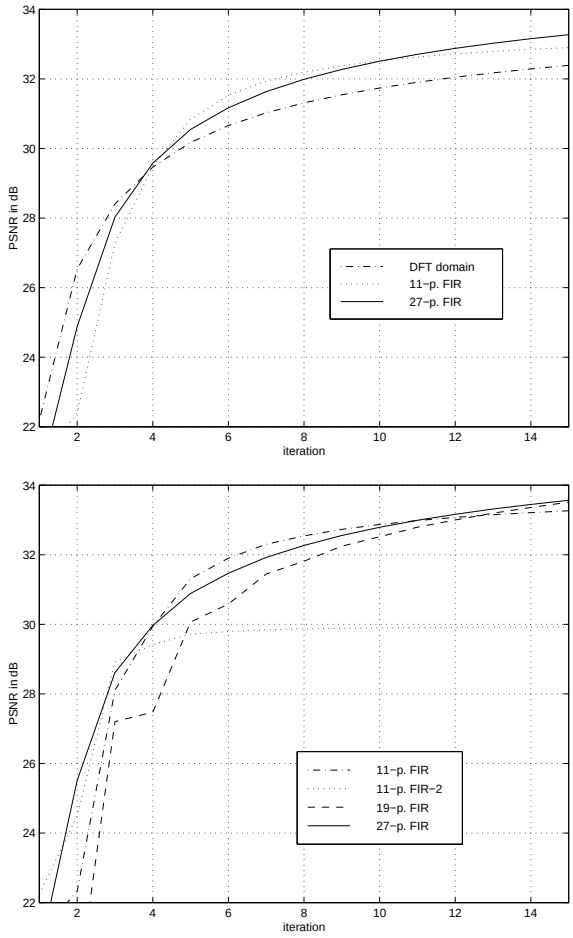

Figure 2: Evolution of PSNR of the reconstruction error.

[3] A. Sharaf and F. Marvasti, "Motion compensation using spatial transformations with forward mapping," *Signal Process., Image Commun.*, vol. 14, pp. 209–227, 1999.

[4] P. Combettes, "The foundations of set theoretic estimation," *Proc. IEEE*, vol. 81, no. 2, pp. 182–208, Feb. 1993.

[5] R. Stasiński and J. Konrad, "POCS-based image reconstruction from irregularly-spaced samples," in *Proc. IEEE Int. Conf. Image Processing*, Sept. 2000, vol. II, pp. 315–318.

[6] R. Stasiński and J. Konrad, "POCS reconstruction of stereoscopic views," in *Proc. Int. Conf. on Augmented, Virtual Environments and Three-Dimensional Imaging*, May 2001, pp. 41–44.

[7] E. Dubois, "The sampling and reconstruction of time-varying imagery with application in video systems," *Proc. IEEE*, vol. 73, no. 4, pp. 502–522, Apr. 1985.

[8] K.D. Sauer and J.P. Allebach, "Iterative reconstruction of band-limited images from nonuniformly spaced samples," *IEEE Trans. Circuits Syst.*, vol. 34, no. 12, pp. 1497–1506, Dec. 1987.